

Recent Advances in Binary Star Formation Using SPH

Matthew R. Bate

Institute of Astronomy, Madingley Road, Cambridge CB3 0HA, United Kingdom

E-mail: mbate@ast.cam.ac.uk

We review recent advances in the study of binary star formation that have been made using the smoothed particle hydrodynamics technique.

1. INTRODUCTION

The Smoothed Particle Hydrodynamics (SPH) numerical method was introduced by Lucy [20] and Gingold and Monaghan [21]. Its first application was in the field of star formation, where it was used to study whether or not a rapidly-rotating polytrope could undergo fission to form a close binary system [20, 22]. Since this initial application, SPH has been widely used in the study of star formation, for example [23, 31, 29, 17, 35, 10, 7, 25, 34, 2, 28, 33, 39, 16].

SPH has many attributes which make it particularly well suited to the study of star formation. SPH is Lagrangian and does not require a computational grid. Thus, it can efficiently follow problems with large density contrasts since computational effort is not wasted simulating the low-density regions. Also, recent SPH implementations [19, 26, 9, 32] use spatially and temporally varying smoothing lengths so that the resolution increases automatically with increasing density; the complex multi-grid and adaptive-grid schemes that are used for finite difference methods are avoided.

In this proceedings, we review some of the recent advances in the study of binary star formation that have been made using SPH. In Section 2, we discuss the importance of always resolving the Jeans mass in numerical studies of self-gravitating gas. While this has been demonstrated using various types of hydrodynamic code, we concentrate specifically on the problems that can arise if this criterion is not obeyed with SPH. In Section 3, we demonstrate that, for the first time, it is now possible to perform three-dimensional hydrodynamic calculations which follow the collapse of a molecular cloud core to stellar densities. These calculations are performed with SPH. Finally, in Section 4, we discuss how SPH has been used to study the evolution of a protobinary system as it accretes from an infalling gaseous envelope and how this work can lead to predictions of the properties of binary stars.

2. THE IMPORTANCE OF RESOLVING THE JEANS MASS

It has recently been realised that it is important that the Jeans mass/length is always resolved during a hydrodynamical calculation. This has been demonstrated

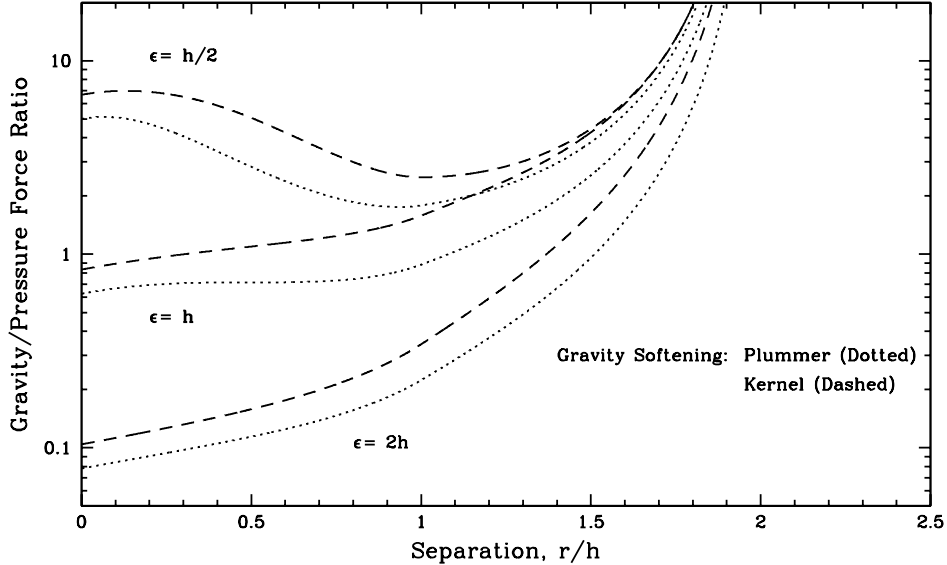


FIG. 1. The ratio of the gravitational force to pressure force between two SPH particles in a Jeans-mass clump of gas of radius $R = h$. The gravitational softening length is ϵ and the hydrodynamic smoothing length is h .

both with SPH [8, 40] and with grid-based codes [37, 38, 14]. If this criterion is not obeyed, artificial fragmentation can be induced, or fragmentation can be inhibited. Essentially this is because when the resolution length/mass approaches the Jeans length/mass, collapse is artificially delayed due to viscous forces, softening of gravitational forces, or a combination of both. A good example is the collapse of an isothermal filament [37]. Such a filament should collapse without limit to a filamentary singularity without fragmenting. However, if the collapse perpendicular to the major-axis is delayed, small density perturbations along the filament may have enough time to grow to non-linear amplitudes and fragments may form along the bar.

Bate & Burkert [8] first demonstrated the need for the Jeans mass criterion using self-gravitating SPH calculations. With SPH, the problem can be understood by considering the gravitational and pressure forces between two particles within a marginally Jeans-stable clump of gas of radius $R \approx h$ (Figure 1). SPH codes typically soften the gravitational forces between neighbouring particles, using either the Plummer force law or kernel softening [21, 26, 9]. The characteristic gravitational softening length, ϵ , may or may not be equal to the SPH hydrodynamic smoothing length, h , depending on the specific implementation. If $\epsilon = h$, the ratio of the gravitational and pressure forces between two particles is approximately constant for particle with separations $\lesssim h$. Thus, a Jeans-unstable clump of gas will collapse, while a Jeans-stable clump will be supported. However, although the ratio of the gravitational and pressure forces is approximately independent of the separation of the particles, the magnitude of the gravitational force decreases with separation due to the softening. Thus, while a Jeans-unstable clump of gas with a size much

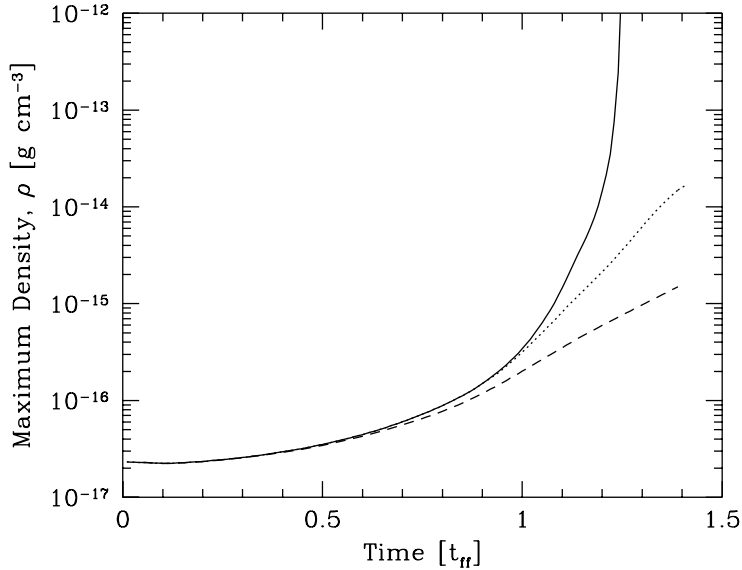


FIG. 2. Maximum density versus time for during the collapse of a molecular cloud core [8]. Three calculations were performed using SPH with $\epsilon = h$. The smoothing lengths were allowed to vary with time and space freely (solid line) or subject to a minimum length of 5% (dotted line) or 10 % (dashed line) of the initial cloud radius. When the minimum Jeans length in the calculation is less than or approximately equal to the smoothing/softening length, the collapse is delayed.

larger than the resolution length, h , will collapse at the correct rate, the collapse of clumps with a size $\approx h$ will be delayed. This is demonstrated in Figure 2.

Unfortunately, the effect is not always limited to a simple delay of the collapse. Given the right problem, artificial fragmentation can be induced (such as with the filament described above), or inhibited. In Figure 3 we show how the collapse of a particular molecular cloud core with an initial $m = 2$ density perturbation results in a binary protostellar system with a bar of gas between them. This calculation was performed with 8×10^4 particles, enough to resolved the Jeans mass/length until after the binary had formed. However, performing the same calculation with 1×10^4 particles gives a different result: a single, dense bar of gas without the binary. In this calculation, the Jeans mass becomes unresolved before $t = 1.20$ and the collapse of each of the two over-dense regions resulting from the original $m = 2$ density perturbation is delayed. The collapse of the larger-scale elongated region, however, continues, leading to the formation of a bar rather than a binary.

It is important to note that, with SPH, the effect of not resolving a Jeans mass also depends on the way the gravitational softening and hydrodynamic smoothing are implemented! If $\epsilon < h$, the ratio of the gravitational to pressure forces between two particles increases with decreasing separation (Figure 1). This may lead to an instability in which a group of particles within a Jeans-stable clump collapse artificially. As demonstrated in Figure 5, this can lead to artificial fragmentation. Alternately, if $\epsilon > h$, the pressure forces between particles within a Jeans-unstable clump may exceed the gravitational forces and the clump will be artificially supported against collapse.

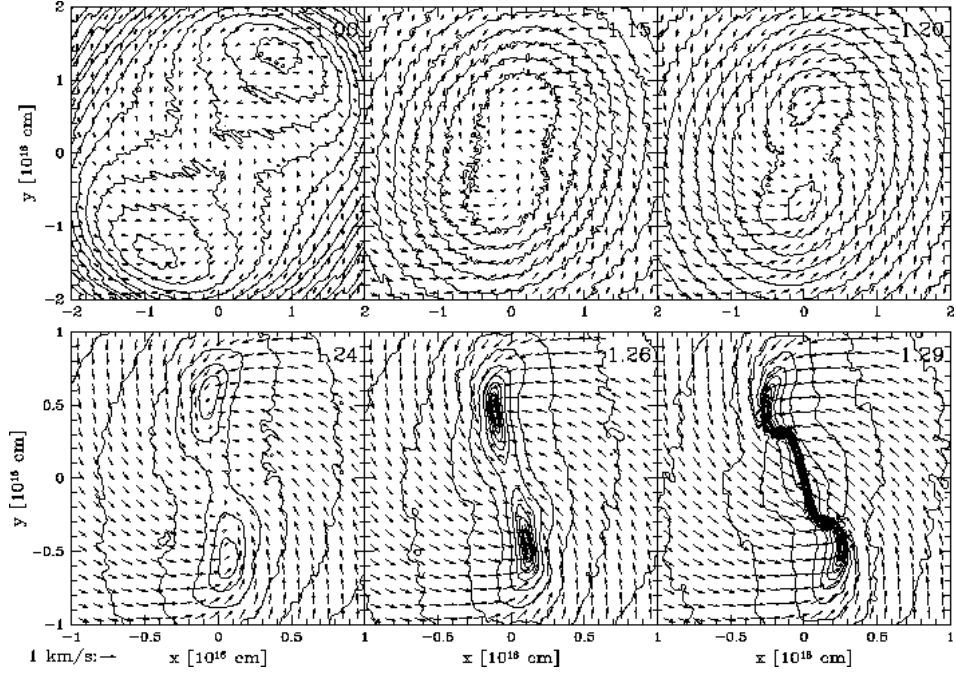


FIG. 3. Collapse and fragmentation of a molecular cloud core to form a binary [8]. The initial cloud had an initial 10% $m = 2$ density perturbation. The local Jeans mass/length is unresolved inside the thick density contour. The calculation was performed with 8×10^4 particles.

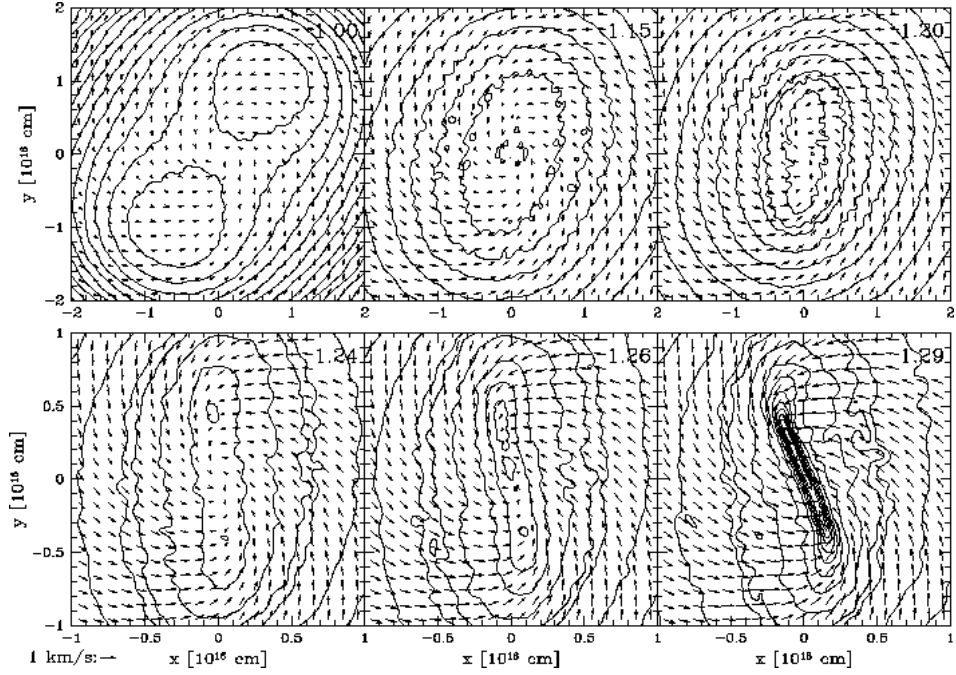


FIG. 4. Same as Figure 3, except that the calculation was performed with 1×10^4 particles. When $t \gtrsim 1.20$, the region within which the binary formed in the 8×10^4 -particle calculation becomes unresolved, collapse of the two over-dense regions is delayed, and the calculation eventually produces a dense bar instead of a binary.

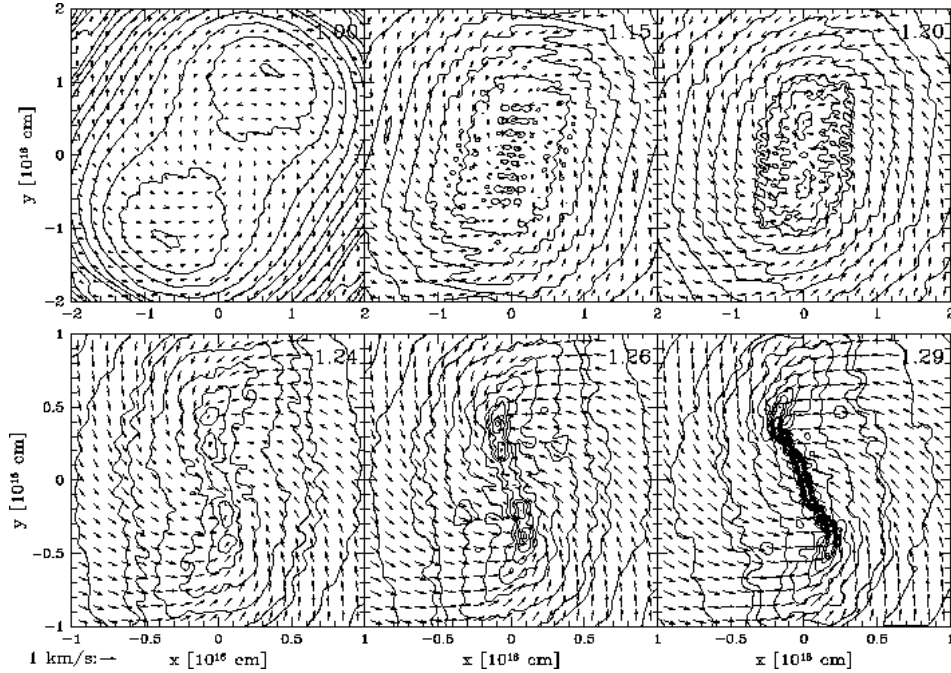


FIG. 5. Same as Figure 4, except that the calculation was performed with $\epsilon = 1.0 \times 10^{14}$ cm (i.e. $e < h$) instead of $e = h$. When the local Jeans-mass becomes unresolved ($t \gtrsim 1.20$), the calculation becomes susceptible to artificial fragmentation. Instead of a binary being formed, each of the two over-dense regions undergoes binary fragmentation so that the final result is a quadruple system.

Clearly, the best SPH implementation is one where $\epsilon = h$ always. In this case, collapse of Jeans-unstable clumps with a size similar to that of the resolution length will still be delayed, but the possibilities of artificial collapse within Jeans-stable clumps or the supporting of Jeans-unstable clumps against collapse are eliminated. Then, in order to avoid the collapse of Jeans-unstable clumps being delayed significantly, enough particles should be used so that the Jeans length/mass is always resolved.

How many particles are necessary to ensure that the Jeans length/mass is resolved? With SPH, the spatial resolution is given by the smoothing length which is usually variable in time and space. The smoothing lengths are set by ensuring that each particle contains a certain number of neighbours, N_{neigh} , or equivalently a fixed mass, within two smoothing lengths. Thus, in contrast to a grid-based code which has spatially-limited resolution, SPH has mass-limited resolution which *automatically* gives greater spatial resolution in regions of higher density. Therefore, with SPH, it is necessary to ensure that the minimum resolvable mass is always less than the Jeans mass. In practice, Bate & Burkert found that a Jeans mass should always be represented by at least $\approx 2N_{\text{neigh}}$ particles.

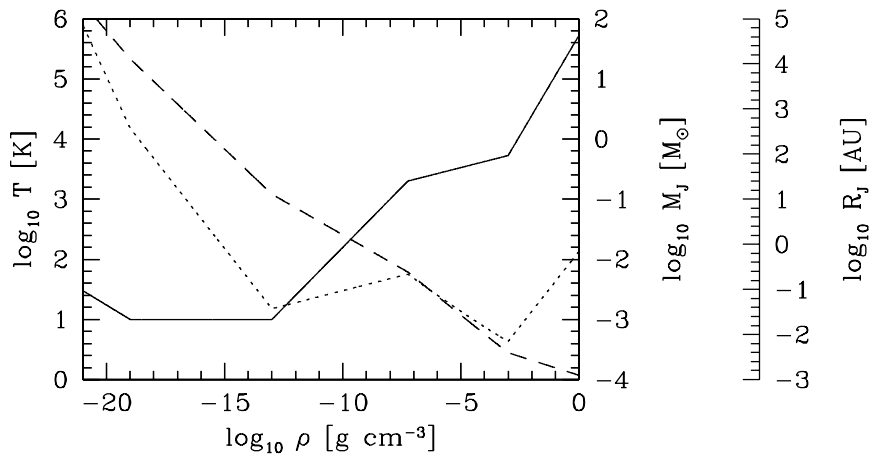


FIG. 6. The gas temperature T (solid line), Jeans mass M_J (dotted line), and Jeans radius R_J (dashed line), as a function of density in a collapsing molecular cloud core (adapted from Tohline [36]). The minimum Jeans mass of $\approx 4 \times 10^{-4} M_\odot$ occurs at a density of $\sim 10^{-13} \text{ g cm}^{-3}$.

3. COLLAPSE OF A MOLECULAR CLOUD TO STELLAR DENSITIES

The mass-limited resolution of SPH is ideal for studying the collapse and fragmentation of molecular cloud cores because there is a minimum Jeans mass in the problem (Figure 6). By contrast, there is no minimum Jeans length. This is a problem for grid-based codes which must resort to nested or adaptive grids [15, 37, 38]. With SPH, if the number of particles used is sufficient to resolve the minimum Jeans mass, a calculation can be followed to arbitrary densities with the required spatial resolution given automatically with increasing density.

Recently, this ability of SPH was used to perform the first three-dimensional calculations ever to follow the collapse of a molecular cloud core to stellar densities [4]. The calculations followed the collapse of an initially uniform-density molecular cloud core of mass $M = 1 M_\odot$ and radius $R = 7 \times 10^{16} \text{ cm}$.

The minimum resolvable mass in the SPH code was $\approx 2N_{\text{neigh}} = 100$ particles. Thus, to enable the minimum Jeans mass during the calculation ($\approx 4 \times 10^{-4} M_\odot$) to be resolved, the calculation used 3×10^5 equal-mass particles.

The code did not include radiative transfer. Instead, to model the behaviour of the gas during the different phases of collapse, a piece-wise polytropic equation of state, $P = K\rho^\gamma$, was used, where P is the pressure, ρ is the density, K gives the entropy of the gas, and the ratio of specific heats, γ , was varied as

$$\gamma = \begin{cases} 1 & \rho \leq 1.0 \times 10^{-13} \\ 7/5 & 1.0 \times 10^{-13} < \rho \leq 5.7 \times 10^{-8} \\ 1.15 & 5.7 \times 10^{-8} < \rho < 1.0 \times 10^{-3} \\ 5/3 & \rho > 1.0 \times 10^{-3} \end{cases} \quad (1)$$

where the densities are in g cm^{-3} (see Figure 6). The values of γ and the transition densities were derived from Tohline [36]. The variable value of γ mimics the following behaviour of the gas. The collapse is isothermal ($\gamma = 1$) until the gas becomes optically thick to infrared radiation at $\rho \approx 10^{-13} \text{ g cm}^{-3}$, beyond which

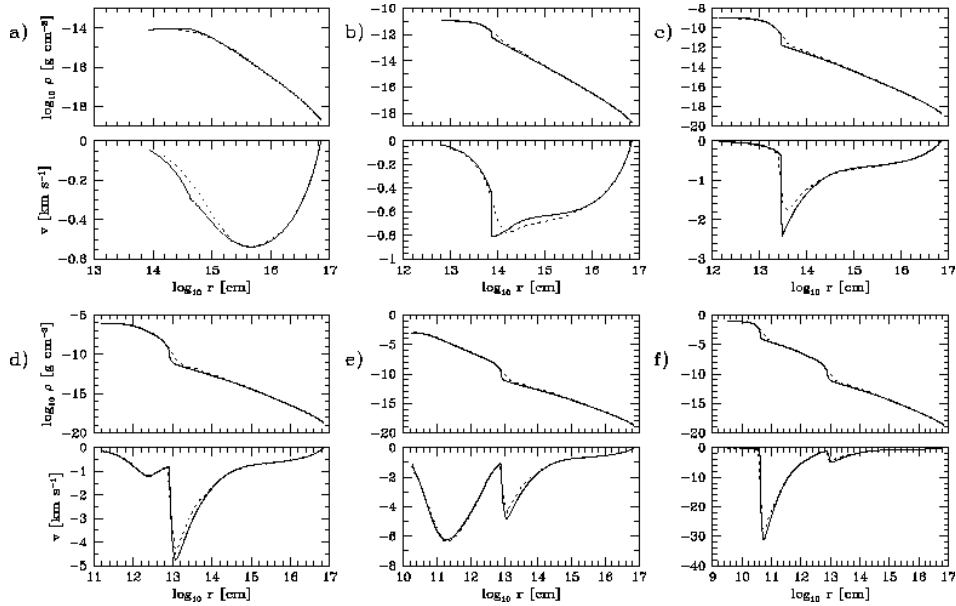


FIG. 7. Radial density and velocity profiles of the collapsing molecular cloud core with the one-dimensional grid code (solid) and the three-dimensional SPH code (dotted). The profiles are compared when the central density in each calculation is a) 10^{-14} , b) 10^{-11} , c) 10^{-9} , d) 10^{-6} , e) 10^{-3} , and f) 10^{-1} g cm^{-3} .

$\gamma = 7/5$ (appropriate for a diatomic gas). When the gas reaches a temperature of ≈ 2000 K ($\rho = 5.7 \times 10^{-8}$ g cm^{-3}), molecular hydrogen begins to dissociate and the temperature only slowly increases with density. In this phase $\gamma = 1.15$ is used to model *both* the decreasing mean molecular weight and the slow increase of temperature with density, the latter of which has an effective $\gamma \approx 1.10$. Finally, when the gas has fully dissociated ($\rho \approx 10^{-3}$ g cm^{-3}), the gas is monatomic and $\gamma = 5/3$. The value of K is defined such that when the gas is isothermal, $K = c_s^2$ with $c_s = 2.0 \times 10^4$ cm s^{-1} , and when γ changes the pressure is continuous.

3.1. Collapse of an initially-static cloud

To test that the above equation of state captures the important elements of the gas's behaviour, spherically-symmetric, one-dimensional (1-D), finite-difference calculations were performed of the collapse of an initially-static molecular cloud core with the above parameters and equation of state. The results are shown in Figure 7 (solid line). These results are in good agreement with the results from 1-D calculations incorporating radiative transfer (e.g. Larson 1969; Winkler & Newman 1980a, b).

The three-dimensional (3-D) SPH code was also tested on the same problem to check that the SPH code can indeed accurately resolve the collapse down to stellar densities (Figure 7, dotted line). There is excellent agreement between the results from the 1-D finite-difference code and those from the 3-D SPH code.

3.2. Collapse of a rotating cloud

Three-dimensional calculations are required if the molecular cloud core is rotating. In Figures 8 to 11 we present results from the collapse of a cloud core which is

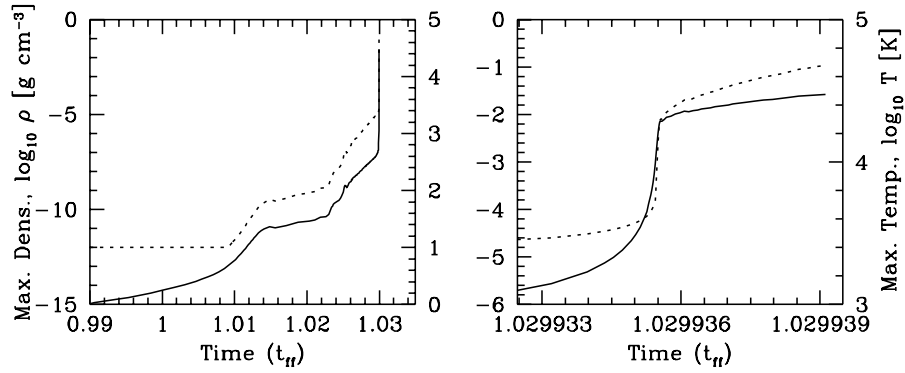


FIG. 8. Maximum density (solid line) and maximum temperature (dotted line) versus time for the collapsing molecular cloud core. Time is given in units of the initial free-fall time ($t_{ff} = 1.785 \times 10^{12}$ s). The right graph has expanded axes to show the second collapse phase in greater detail.

identical to that in the previous section, but which is initially in solid-body rotation with angular frequency $\Omega = 7.6 \times 10^{-14}$ rad s $^{-1}$. Thus, the ratio of rotational energy to the magnitude of the gravitational potential energy is $\beta = 0.005$ (i.e. the cloud is rotating quite slowly).

The evolution of the calculation is as follows (Figure 8). The initial collapse is isothermal. When the density surpasses 10^{-13} g cm $^{-3}$, the gas in the center is assumed to become optically thick to infrared radiation and begins to heat ($t =$

FIG. 9. A time sequence showing the density in the plane perpendicular to the rotation axis during the dynamic, rotational, bar instability of the first hydrostatic core. The panels cover the period from $t \approx 1.023 - 1.030 t_{ff}$. See also the MPEG animation on this CD-ROM: batel.mpg.

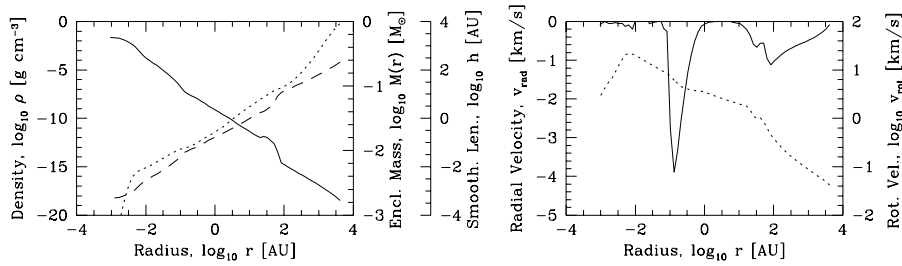


FIG. 10. The state of the system at the end of the calculation. The left graph gives the density (solid line) and smoothing length (dashed line) as a function of radius and the mass enclosed within radius r of the center of the stellar core (dotted line). The right graph gives the radial (solid line) and rotational (dotted line) velocities as functions of radius from the center of the stellar core. The densities, smoothing lengths and velocities are the mean values in the plane perpendicular to the rotation axis and through the stellar core. The stellar core ($r < 0.004$ AU), inner circumstellar disc ($0.004 < r < 0.1$ AU), region undergoing the second collapse ($0.1 < r < 1$ AU), outer circumstellar disc formed from the first core ($1 < r < 60$ AU), and isothermal collapse region ($r > 60$ AU) are clearly visible.

$1.009 t_{\text{ff}}$). The heating stops the collapse at the center and the first hydrostatic core is formed ($t = 1.015 t_{\text{ff}}$) with maximum density $\approx 2 \times 10^{-11} \text{ g cm}^{-3}$, mass $\approx 0.01 M_{\odot}$ ($\approx 3 \times 10^3$ particles), and radius ≈ 7 AU. As the first core accretes, its maximum density only slowly increases at first. However, the first core is rapidly rotating, oblate, and has $\beta \approx 0.34 > 0.274$, making it dynamically unstable to the growth of non-axisymmetric perturbations [17, 27]. At $t \approx 1.023 t_{\text{ff}}$, after about 3 rotations, the first core becomes violently bar-unstable and forms trailing spiral arms (Figure 9). This leads to a rapid increase in maximum density (Figure 8) as angular momentum is removed from the central regions of the first core (now a disc with spiral structure) by gravitational torques ($t = 1.023 - 1.030 t_{\text{ff}}$). An MPEG animation of this bar instability is provided on this CD-ROM (bate1.mpg). When the maximum temperature reaches 2000 K, molecular hydrogen begins to dissociate, resulting in a rapid second collapse to stellar densities ($t = 1.030 t_{\text{ff}}$). The collapse is again halted at a density of $\approx 0.007 \text{ g cm}^{-3}$ with the formation of the second hydrostatic, or stellar, core. The initial mass and radius of the stellar core are $\approx 0.0015 M_{\odot}$ ($\approx 5 \times 10^2$ particles) and $\approx 0.8 R_{\odot}$, respectively. Finally, an inner circumstellar disc begins to form around the stellar object, within the region undergoing second collapse. The calculation is stopped when the stellar object has a mass of $\approx 0.004 M_{\odot}$ ($\approx 1.2 \times 10^3$ particles), the inner circumstellar disc has extended out to ≈ 0.1 AU, and the outer disc (the remnant of the first hydrostatic core) contains $\approx 0.08 M_{\odot}$ ($\approx 2.4 \times 10^4$ particles) and extends out to ≈ 70 AU. Note that the massive outer disc forms *before* the stellar core. This final state is illustrated in Figures 10 and 11. If the calculation was evolved further, the inner circumstellar disc would continue to grow in radius as gas with higher angular momentum fell in. Eventually, the inner disc would meet the outer disc with only a small molecular dissociation region between the two.

3.3. Close binary stellar systems

The ability to perform three-dimensional calculations which follow the collapse of molecular cloud cores to stellar densities allows us to study the formation of close ($\lesssim 1$ AU) binary stellar systems. Currently, there is no accepted mechanism

FIG. 11. The state of the system at the end of the calculation (not a time sequence). The upper six panels give the density in the plane perpendicular to the rotation axis and through the stellar core. The lower six panels give the density in a section down the rotation axis. In each case, the six consecutive panels give the structure on a spatial scale that is 10 times smaller than the previous panel to resolve structure from 3000 AU to $\approx 0.2 R_{\odot}$. The remnant of the first hydrostatic core (now a disc with spiral structure), the inner circumstellar disc, and the stellar core are all clearly visible. The logarithm of the density is plotted with the maximum and minimum densities (in g cm^{-3}) given under each panel.

for forming close binaries; the proposal that close binary systems form via the fission of a rapidly-rotating protostellar object has been discredited by studies of rapidly-rotating polytropes [17]. Although fission itself appears not to operate, it is possible that fragmentation can still occur due to the growth of non-axisymmetric perturbations in rotationally-supported objects. Only two studies have looked at this possibility in detail [13, 11], and the latter of these finds that fragmentation of a massive circumstellar disc on scales ($\lesssim 1$ AU) may be possible. However, in both these studies, only the region inside the first hydrostatic core was modelled and the initial conditions were chosen somewhat artificially. The ability to perform three-dimensional calculations which follow the collapse of molecular cloud cores to stellar densities now allows us to study the formation of close binaries from the collapse of larger-scale (≈ 10000 AU) molecular cloud cores.

4. THE EVOLUTION OF AN ACCRETING PROTOBINARY SYSTEM

The favoured mechanism for the formation of most binary stellar systems is the fragmentation of a collapsing molecular cloud core. Fragmentation has been studied numerically for ≈ 20 years. These calculations appear to show that it is possible to form binaries with similar properties to those that are observed via fragmentation. However, they have not allowed us to predict the fundamental properties of stellar systems such as the fraction of stellar systems which are binary or the properties of binary systems (e.g. the distributions of mass ratios, separations, and eccentricities and the properties of discs in pre-main-sequence systems).

There are two primary reasons for this lack of predictive power. First, the results of fragmentation calculations depend sensitively on the initial conditions, which are poorly constrained. The second problem is that of accretion. Fragmentation calculations are typically stopped soon after the fragmentation occurs, when the binary or multiple protostellar system contains only a small fraction of the total mass of the original cloud [12, 11]. However, because much of the gas contained in the original cloud still has to fall on to the system and be accreted, the final properties of the stellar system are unknown. Following the calculation significantly beyond the point at which fragmentation occurs is extremely computationally intensive. Thus, it is impossible to perform the number of calculations that are required to predict the statistical properties of binary stellar systems – even if we knew the distribution of the initial conditions. On the other hand, if we can overcome this second difficulty, we can make theoretical predictions about the properties of binary stars and, by comparing these predictions to the observed properties of binary systems, we may be able to better constrain the initial conditions for star formation.

4.1. The Effects of Accretion on a Protobinary System

Using SPH, Bate & Bonnell [6] studied and quantified how the properties of a binary system are affected by the accretion of a small amount of gas from an infalling gaseous envelope. They found that the effects depend primarily on the specific angular momentum of the gas and the binary's mass ratio (see also [1, 3]). Generally, accretion of gas with low specific angular momentum decreases the mass ratio and separation of the binary, while accretion of gas with high specific angular momentum increases the separation and drives the mass ratio toward unity. From these results, they predicted that closer binaries should have mass ratios that are

FIG. 12. The dependence of the distribution of gas around an accreting protobinary system on the specific angular momentum of the infalling gas (increasing from left-to-right and downward). For gas with low specific angular momentum, only the primary forms a circumstellar disc and the secondary accretes a small amount of gas via a Bondi-Hoyle-type accretion stream. For gas with intermediate angular momentum, both the primary and secondary form circumstellar discs. For gas with high angular momentum, two circumstellar discs and a circumbinary disc are formed. Finally, for the case with the highest angular momentum, all the infalling gas settles into a circumbinary disc. The binary has a mass ratio of $q = 0.6$ and the primary is on the right.

biased toward equal masses compared to wider systems, since the gas which falls on to a closer system is likely to have more specific angular momentum, relative to the binary, than for a wider system.

They also studied the process of disc formation around an accreting protobinary system and found that for each protostar, a circumstellar disc was only formed if the specific angular momentum of the infalling gas was greater than the specific orbital angular momentum of that protostar about the centre of mass of the binary (Figure 12). This is because, to be captured by one of the protostars, the gas must achieve the same specific orbital angular momentum as that of the protostar. If the gas has more specific angular momentum initially, some of its angular momentum goes into forming a disc around the protostar. However, if it has less specific angular momentum initially, there is no excess angular momentum to form a circumstellar disc, and it must gain angular momentum even to be captured by the protostar. In this case, the infalling gas gains angular momentum as it falls on to the protostar in a Bondi-Hoyle-type accretion stream. In practice, this means that a circumstellar disc is almost always formed around the primary, but the secondary does not have a circumstellar disc unless the infalling gas has more specific angular momentum than some critical value. In a similar way, the formation of a circumbinary disc only begins when the specific angular momentum of the infalling gas is great enough for

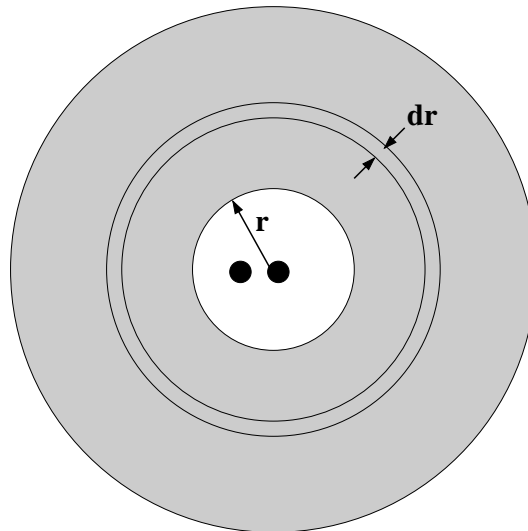


FIG. 13. The model for studying the evolution of a protobinary system that forms within a collapsing molecular cloud core and is built up to its final mass by accreting the remaining gas as it falls on to the binary.

the gas to form a circular orbit at a radius greater than that of the secondary from the centre of mass of the binary.

4.2. Development of a Protobinary Evolution Code

Using the quantitative results of Bate & Bonnell [6], Bate [5] developed a protobinary evolution (PBE) code which follows the evolution of a protobinary system as it accretes from its initial to its final mass, but does so in far less time than would be required for a full hydrodynamic calculation.

This code is based on the following model for the formation of binary stellar systems (Figure 13). The model begins with a molecular cloud core of known initial density and angular momentum profile. It is assumed that this cloud begins to collapse and that a ‘seed’ binary system is formed at the centre, presumably via some sort of fragmentation. The ‘seed’ binary has mass ratio $q \leq 1$, separation a , and is assumed to have a circular orbit. Its initial state consists of only a small fraction of the total mass of the core and is assumed to have formed from the gas that was originally contained within a sphere of radius r , at the centre of the initial cloud (Figure 13). For the results presented in this proceedings, the separation of the ‘seed’ binary is set by assuming that the angular momentum of the gas from which the binary forms is equal to the orbital angular momentum of the binary.

Subsequently, the binary accretes the remainder of the initial cloud (which falls on to the binary) and the binary’s properties evolve due to the accretion. This evolution is calculated by taking a thin shell of gas of thickness dr (Figure 13), surrounding the sphere from which the binary was formed, dividing the shell into small elements of gas, and calculating the effect that each element of gas has on the protobinary when it is accreted (using the results of Bate & Bonnell [6]). The binary’s parameters (masses and separation) are updated, and the next shell of gas is considered until the whole cloud is accreted on to the binary. The amount of gas which settles into a circumbinary disc is also recorded. In this way, the code

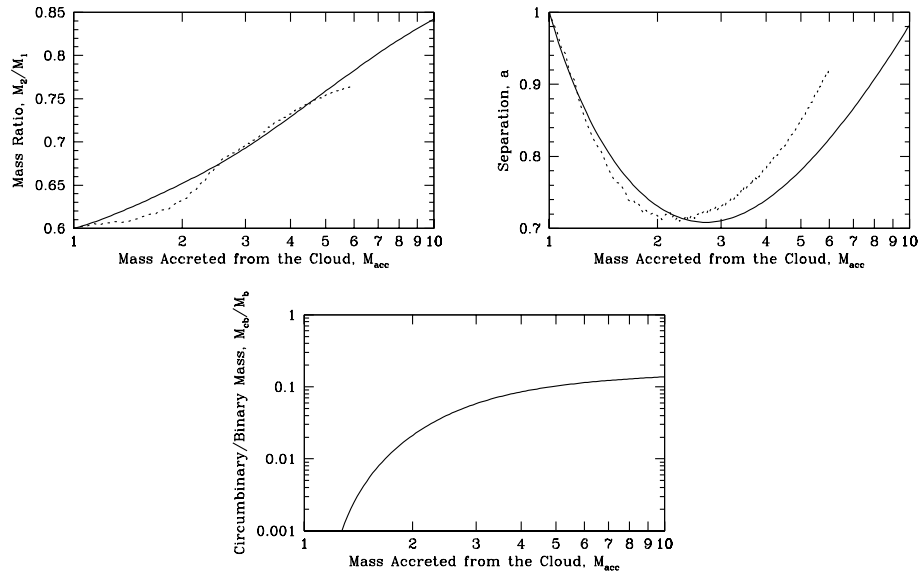


FIG. 14. First comparison of the results from the protobinary evolution (PBE) code (solid lines) with those from a full SPH calculation (dotted lines). The graphs show the evolution of a protobinary system that was formed in the centre of a collapsing molecular cloud core which initially had a uniform-density profile and was in solid-body rotation. The evolution of the (a; upper left) mass ratio, (b; upper right) separation, (c; lower) ratio of mass in a circumbinary disc to that of the binary are plotted as the binary accretes gas from the infalling envelope.

calculates the evolution of the binary from its initial to its final state when all of the original cloud's gas is contained either in one of the two stars or their surrounding discs.

4.3. Testing the Protobinary Evolution Code

To test how accurately the PBE code describes the evolution of a 'seed' binary as it accretes from its initial to its final mass, the PBE results were compared to those from full SPH calculations. Two test cases were performed. The first followed the formation of a binary system from the collapse of an initially uniform-density, spherical molecular cloud core in solid-body rotation. The 'seed' binary was assumed to have a mass ratio of $q = 0.6$ and a mass of $1/10$ the initial cloud mass. The second test case was similar, except that the progenitor cloud was centrally-condensed with a $1/r$ -density distribution and the cloud had a total mass of only 5 times the 'seed' binary's mass. A full discussion of the test cases is given by [5].

4.3.1. Test Case 1

The evolution of the mass ratio, separation and amount of gas in the circumbinary disc are given for the PBE code and for a full SPH calculation in Figure 14. The curves are given as functions of the amount of gas that has fallen on to the binary, M_{acc} , relative to the binary's initial mass. In addition, an MPEG animation of the SPH calculation is included on this CD-ROM as `bate2.mpg`. The CPU time required to evolve the SPH calculation until the entire cloud falls on to the binary is prohibitively long, which, after all, is the reason that the PBE code was developed

in the first place. It takes ≈ 60 orbits for the binary to increase its mass by a factor of 6 (i.e. $\approx 60\%$ of the total cloud was accreted). The SPH calculation took ≈ 5 months on a 170 MHz Sun Ultra workstation with a GRAvity-PipE (GRAPE) board used to calculate the gravitational forces and neighbouring SPH particles. The evolution with the PBE code took a few seconds!

Although the SPH calculation did not run to completion, we can compare the evolution as the binary's mass increases by a factor of 6 (Figure 14). Generally, there is good agreement between the PBE and SPH codes. The mass ratio is predicted to within 5% over the entire evolution and the separation to within 15%. In fact, as discussed in [5], the small differences between the PBE and SPH results reflect unphysical treatment of the circumstellar discs by the SPH code rather than a problem with the PBE code. For example, the slower rate of increase of the mass ratio initially is due to the circumsecondary disc not being resolved correctly in the SPH calculation, and the larger separation when $M_{\text{acc}} \gtrsim 3$ is due to unphysically-rapid viscous evolution of the circumstellar discs which transfers angular momentum into the binary's orbit too quickly. The greatest difference between the PBE and SPH results is that the PBE code predicts that a circumbinary disc should be formed around the binary whereas no circumbinary disc is formed in the SPH calculation. This is due to the larger separation of the binary when $M_{\text{acc}} \gtrsim 3$ and the large shear viscosity in the SPH calculation.

4.3.2. Test Case 2

Unlike test case 1, the PBE code predicts that a massive circumbinary disc should be produced very early in the evolution of test case 2. Thus, test case 2 provides a better test of how well the PBE code predicts the formation of a circumbinary disc and its evolution. We note that, although the PBE code records the amount of gas which settles into a circumbinary disc, it does not attempt to take account of the interaction between the binary and the circumbinary disc. In reality, this interaction is expected to result in the transfer of angular momentum from the orbit of the binary into the gas of the circumbinary disc and, hence, in a smaller separation. Furthermore, if the separation decreases, more of the infalling gas would be expected to settle into the circumbinary disc and, for the same increase in the binary's mass, the mass ratio should increase more rapidly because the gas has a greater specific angular momentum relative to that of the binary. Thus, if a massive circumbinary disc is formed, the PBE code is expected to over-estimate the binary's separation, under-estimate the mass in the circumbinary disc, and slightly under-estimate the mass-ratio of the binary.

The evolution of the mass ratio, separation and amount of gas in the circumbinary disc are given for test case 2 in Figure 15. An MPEG animation of the SPH calculation is included on this CD-ROM as `bate3.mpg`. To avoid the problems that occurred due to the large shear viscosity in the SPH calculation for test case 1, the SPH calculation here uses a formulation with less shear viscosity (see [5]). As with test case 1, due to the computational cost, the SPH calculations were stopped before all of the gas had fallen on to the binary. The SPH calculation took ≈ 4 months on a 300 MHz Sun Ultra workstation (using a binary tree, not a GRAPE board). During the evolution, the binary performed ≈ 40 orbits and $\approx 60\%$ of the total mass was accreted by the binary or settled into a circumbinary disc.

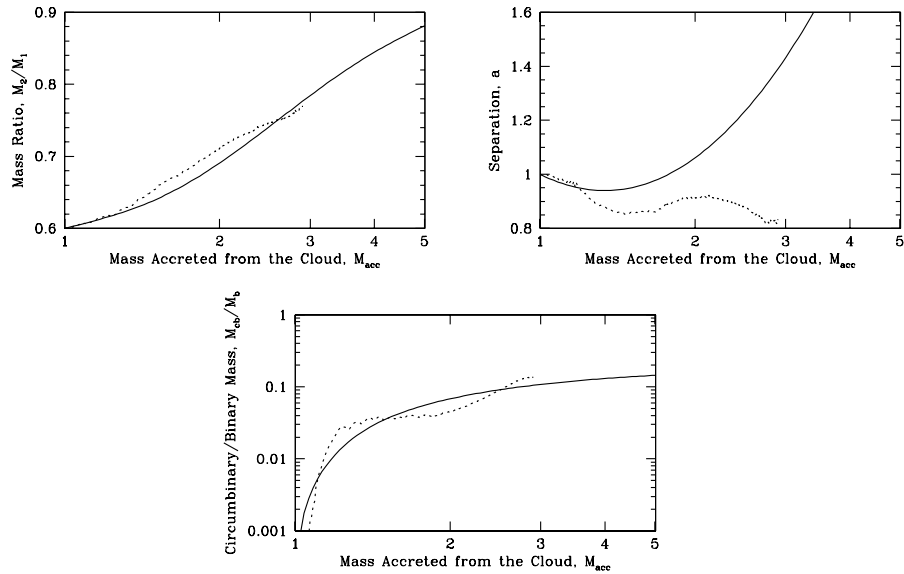


FIG. 15. Same as Figure 14, except that the protobinary system was formed from a molecular cloud core which initially had a density profile of $\rho \propto 1/r$.

The agreement for the evolution of the mass ratio is even better than it was with test case 1 with differences between the PBE and SPH results of $\lesssim 3\%$. The separation follows the prediction of the PBE code to better than 3% until the circumbinary disc begins to form. Once the circumbinary disc attains approximately 5% of the binary’s mass, however, the separation is always smaller than predicted by the PBE code. As described above, this is expected because the PBE code neglects the separation-decreasing effect of the interaction between the binary and the circumbinary disc. This also explains why the PBE code slightly under-estimates the binary’s mass ratio. However, it is pleasing to see that even neglecting the interaction between the binary and the circumbinary disc, the PBE code still predicts the mass of the circumbinary disc to within a factor of 2 of that given by the SPH code during the entire evolution.

4.4. The Evolution of Accreting Protobinary Systems

As we have seen, the PBE code gives a relatively accurate description of the evolution of an accreting protobinary, but does so $\sim 10^6$ times faster than a full hydrodynamic SPH calculation. This allows us to perform many calculations to study how the evolution of a binary as it accretes to its final mass depends on its initial mass ratio and on the properties of the molecular cloud core from which it formed.

As examples, we give the evolution of ‘seed’ binaries that form from two types of molecular cloud core. A greater range of molecular cloud cores is considered in [5]. Figure 16 presents the evolution of binaries formed from molecular cloud cores which had uniform-density and were in solid-body rotation before they began to collapse dynamically. In Figure 17, the molecular cloud cores had radial density

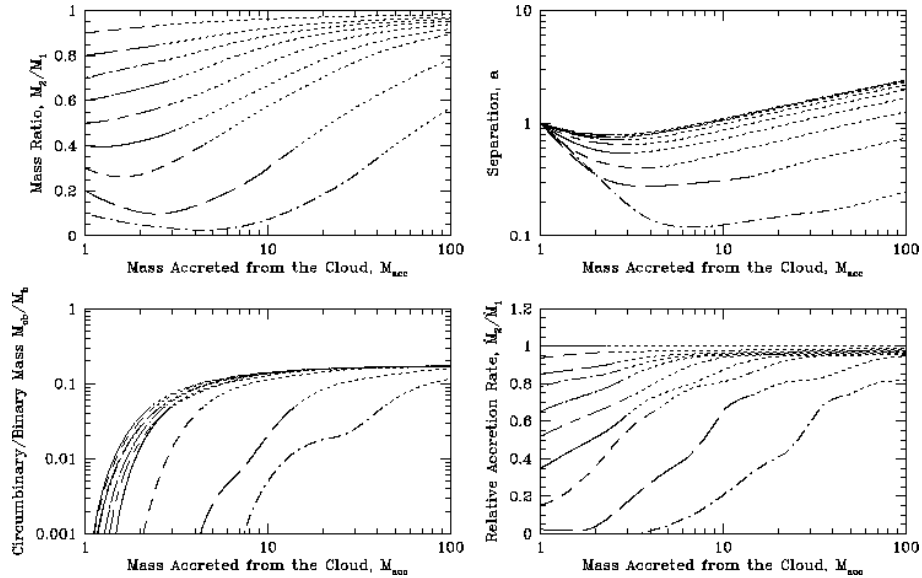


FIG. 16. The evolution of protobinary systems formed in the centre of collapsing molecular cloud cores as they accrete from the gaseous envelope. The initial cores have uniform-density profiles and are in solid-body rotation. The evolution of the mass ratio (a; upper left), separation (b; upper right), and ratio of the circumbinary disc mass to that of the binary (c; lower left), and the relative accretion rate (d; lower right) are given as functions of the amount of gas that has been accreted from the envelope. The evolutionary curves are given for ‘seed’ binary systems with initial mass ratios of $q = 0.1$ to $q = 1.0$, with various different line types and/or widths for each. The curves are all given by a thin dotted line once the circumbinary disc mass exceeds 5% of the binary’s mass. Beyond this point, the binary’s mass ratio and the mass in the circumbinary disc are likely to be under-estimated, and the separation is likely to be over-estimated.

profiles of $\rho \propto 1/r$ with solid-body rotation, initially. Evolutionary curves are provided for ‘seed’ binaries with initial mass ratios ranging from $q = 0.1 - 1.0$.

In all cases, the long-term evolution is towards a mass ratio of unity, since the material that falls in later has higher specific angular momentum relative to that of the binary. Thus, the more the binary accretes relative to its initial mass, the stronger the tendency is for the mass ratio to be driven to unity. Similarly, the more the binary accretes relative to its initial mass, the more likely it is to be surrounded by a circumbinary disc. Note that, in the previous sections, we found that when a massive circumbinary disc is formed, the PBE code tends to over-estimate the separation, and under-estimate the mass of the circumbinary disc and the binary’s mass ratio. Thus, if anything, the evolutionary curves in Figures 16 and 17 tend to under-estimate the binary’s mass ratio and the mass of the circumbinary disc.

4.5. The Properties of Binary Stars

The aim of developing the PBE code was to make it possible to predict some of the properties of binary stars and, by comparing these to the observed properties of binary systems, to constrain the initial conditions for binary star formation.

In order to obtain predictions about the properties of binaries we note that, generally, the initial mass of a ‘seed’ binary is smaller for those binaries with smaller separations. This relationship between a ‘seed’ binary’s mass and its separation is

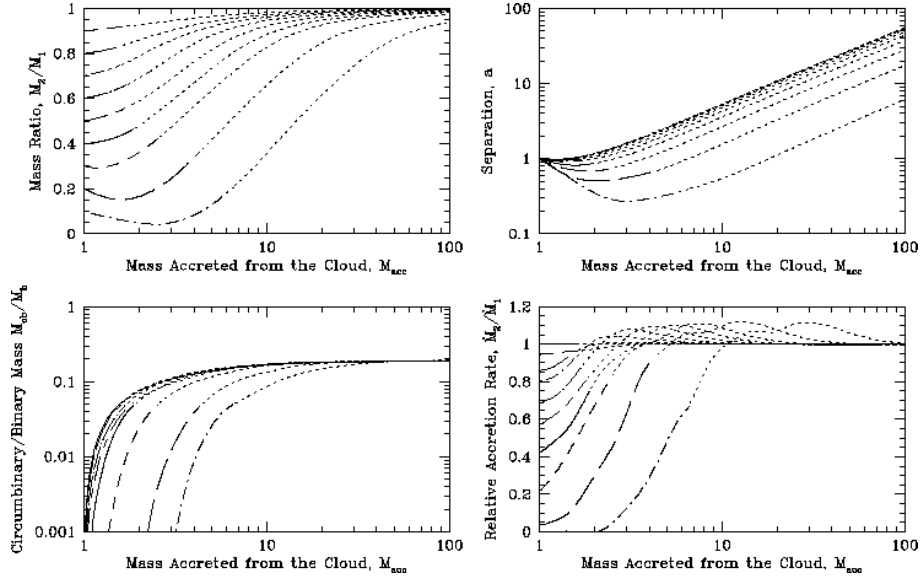


FIG. 17. Same as Figure 16, except that the protobinary systems were formed from a molecular cloud cores which initially had a density profiles of $\rho \propto 1/r$.

observed from fragmentation calculations [12, 11] and is easily understood from a Jeans-mass argument [5]. In order for fragmentation to occur, the Jeans length at the time of fragmentation must be less than or approximately equal to the separation of the binary which is formed. However, for a constant temperature, the Jeans mass depends linearly on the Jeans length. Thus, the smaller the separation of the ‘seed’ binary, the smaller its initial mass. Generally, ‘seed’ binaries with separations $\lesssim 10$ AU are expected to have masses $\approx 0.01M_{\odot}$, while for larger separations, the ‘seed’ mass is expected to increase approximately linearly (i.e. ‘seed’ binaries with separations of 100-1000 AU should have initial masses of $\approx 0.1 - 1.0M_{\odot}$).

This dependence of the initial mass on the separation means that to form binaries with the same final total mass, the closer systems need to accrete more material, relative to their initial mass. Therefore, from the evolutionary curves of Figures 16 and 17, closer systems are more likely to have equal-mass components than wider systems.

This prediction is supported by surveys of main-sequence G-dwarf stellar systems. Duquennoy & Mayor [18] found that the mass-ratio distribution, averaged over binaries with all separations, increases toward small mass ratios. However, there is mounting evidence that the mass-ratio distributions differ between short and long-period systems with the distribution for close binary systems ($P < 3000$ days; $a \lesssim 5$ AU) consistent with a uniform distribution [30, 24]. Thus, relative to wide systems, the close systems are biased toward mass ratios of unity.

The fraction by which the mass of a ‘seed’ binary must be increased in order for its mass ratio to approach unity depends on the conditions in the molecular cloud core. Generally, the less centrally-condensed a core is, the easier it is to form a binary system with a low mass ratio (c.f. Figures 16 and 17). We can use

this dependence of the evolutionary curves on the type of molecular cloud core to attempt to constrain the initial conditions for binary star formation.

Duquennoy & Mayor [18] found that binaries containing G-dwarfs with separations $\gtrsim 30$ AU generally have unequal masses (typically $q \approx 0.3$). Such binaries are likely to have accreted from a few to ten times their initial mass. For uniform-density cores (Figure 16), the observed mass-ratio distribution can easily be obtained. Cores with $\rho \propto 1/r$ result in higher mass ratios than uniform-density cores, but it is still possible to envisage a spectrum of ‘seed’ mass ratios which gives a final mass-ratio distribution which is consistent with the observations of wide binaries.

However, close binaries ($\lesssim 5$ AU) have initial masses of $\approx 0.01M_{\odot}$. Thus, they are expected to have to accrete up to 100 times their initial mass from the infalling gaseous envelope before systems with G-dwarf primaries are obtained, yet the observed mass-ratio distribution is approximately flat (i.e. approximately 1/2 the binaries have $q < 0.5$). It is effectively impossible for cores in solid-body rotation to produce such a mass ratio distribution if they are significantly centrally-condensed (Figure 17). Even with uniform-density cores most of the ‘seed’ binaries would need to have mass ratios $q < 0.1$, which is unlikely.

However, the PBE code only evolves circular binaries whereas most binaries have significant eccentricity [18]. For the same semi-major axis, eccentric binaries have less angular momentum than circular binaries meaning that the clouds from which they formed may be rotating more slowly and, thus, the gas in the envelope may have less angular momentum. This would result in slower evolution toward equal masses for eccentric binaries. Taking the effects of eccentricity into account, it is quite possible that the observed binary mass ratios could be produced by the collapse of molecular cloud cores with radial density profiles less centrally-condensed than $\rho \propto 1/r$. However, even accounting for eccentric binaries, it seems virtually impossible that the observed G-dwarf binary systems could have been formed from molecular cloud cores with density profiles that were more centrally-condensed than $\rho \propto 1/r$.

The above conclusion that closer binaries should have mass ratios that are biased toward unity compared to wider systems with the same total mass is just one of many predictions that may be derived using the PBE code (see [5]). Others include: closer binaries are more likely to have circumbinary discs than wider binaries; brown dwarf companions to solar-type stars should be very rare at separations $\lesssim 5$ AU, but their frequency should increase at larger separations.

5. CONCLUSIONS

The Lagrangian nature of SPH and its inherent ability to provide finer spatial resolution in regions of higher density make it a powerful tool which is ideally suited for studying star formation.

Recent advances in the study of binary star formation that have been made using SPH include: the realisation that it is essential that the Jeans mass is always resolved in numerical studies of self-gravitating gas; the ability to perform three-dimensional hydrodynamic calculations which follow the collapse of a molecular cloud core to stellar densities; the study of the effects of accretion on a protobinary systems and the development of a code which enables the evolution of accreting binary systems to be followed $\sim 10^6$ times faster than a full hydrodynamic calcula-

tion. The latter of these developments has resulted in the first firm predictions of the properties of binary stars for one particular model of binary star formation.

REFERENCES

1. Artymowicz P., 1983, *Acta Astronomica*, 33, 223
2. Artymowicz P., Lubow S. H., 1994, *ApJ*, 421, 651
3. Bate M. R., 1997, *MNRAS*, 285, 16
4. Bate M. R., 1998, *ApJ*, 508, L95
5. Bate M. R., 2000, *MNRAS*, submitted
6. Bate M. R., Bonnell I. A., 1997, *MNRAS*, 285, 33
7. Bate M. R., Bonnell I. A., Price N. M., 1995, *MNRAS*, 277, 362
8. Bate M. R., Burkert A., 1997, *MNRAS*, 288, 1060
9. Benz W., 1990, in Buchler J. R., ed., *The Numerical Modeling of Nonlinear Stellar Pulsations: Problems and Prospects*. Kluwer, Dordrecht, p. 269
10. Bonnell I. A., Bastien P., 1991, *ApJ*, 374, 610
11. Bonnell I. A., Bate M. R., 1994, *MNRAS*, 271, 999
12. Boss A. P., 1986, *ApJS*, 62, 519
13. Boss A. P., 1987, *ApJ*, 319, 149
14. Boss A. P., 1998, *ApJ*, 501, 77
15. Burkert A., Bodenheimer P., 1993, *MNRAS*, 264, 798
16. Chapman S., Pongracic H., Disney M., Nelson A., Turner J., Whitworth A., 1992, *Nature*, 359, 207
17. Durisen R. H., Gingold R.A., Tohline J.E., Boss A.P., 1986, *ApJ*, 305, 281
18. Duquennoy A., Mayor M., 1991, *A&A*, 248, 485
19. Evrard A. E., 1988, *MNRAS*, 235, 911
20. Lucy L., 1977, *AJ*, 82, 1013
21. Gingold R. A., Monaghan J. J., 1977, *MNRAS*, 181, 375
22. Gingold R. A., Monaghan J. J., 1978, *MNRAS*, 184, 481
23. Gingold R. A., Monaghan J. J., 1981, *MNRAS*, 197, 461
24. Halbwachs J. L., Mayor M., Udry S., 1998, in Rebolo R., Martin E. L., Zapatero Osorio M.R., eds., *Brown Dwarfs and Extrasolar Planets (ASP Conf. Ser. 134)*. Brigham Young University, Provo, p. 308
25. Heller, C. H., 1993, *ApJ*, 408, 337
26. Hernquist L., Katz N., 1989, *ApJS*, 70, 419
27. Imamura J. N., Durisen R. H., Pickett B. K., 1999, *ApJ*, in press
28. Larwood J. D., Nelson R. P., Papaloizou J. C. B., Terquem C., 1996, *MNRAS*, 282, 597
29. Lattanzio J. C., Monaghan J. J., Pongracic H., Schwarz M. P., 1985, *MNRAS*, 215, 125
30. Mazeh T., Goldberg D., Duquennoy A., Mayor M., 1992, *ApJ*, 401, 265
31. Miyama S. M., Hayashi C., Narita S., 1984, *ApJ*, 279, 621
32. Monaghan J. J., 1992, *ARA&A*, 30, 543
33. Nelson A. F., Benz W., Adams F. C., Arnett D., *ApJ*, 502, 342
34. Nelson R., Papaloizou J. C., 1993, *MNRAS*, 265, 905
35. Sigalotti L. Di G., Klapp J., *A&A*, 319, 547
36. Tohline, J. E., 1982, *Fund. Cos. Phys.*, 8, 1
37. Truelove J. K., Klein R. I., McKee C. F., Holliman J. H. II, Howell L. H., Greenough J. A., 1997, *ApJ*, 489, L179
38. Truelove J. K., Klein R. I., McKee C. F., Holliman J. H. II, Howell L. H. Greenough J. A., & Woods D. T., 1998, *ApJ*, 495, 821
39. Vanhala, H. A. T., Cameron A. G. W., 1998, *ApJ*, 508, 291
40. Whitworth A. P., 1998, *MNRAS*, 296, 442

This figure "fig09.jpg" is available in "jpg" format from:

<http://arxiv.org/ps/astro-ph/0002202v1>

This figure "fig11.jpg" is available in "jpg" format from:

<http://arxiv.org/ps/astro-ph/0002202v1>

This figure "fig12.jpg" is available in "jpg" format from:

<http://arxiv.org/ps/astro-ph/0002202v1>